SUPPLEMENTAL MATERIAL

The epidermis coordinates auxin-induced stem growth in response to shade

Carl Procko, Yogev Burko, Yvon Jaillais, Karin Ljung, Jeff A. Long, and Joanne Chory

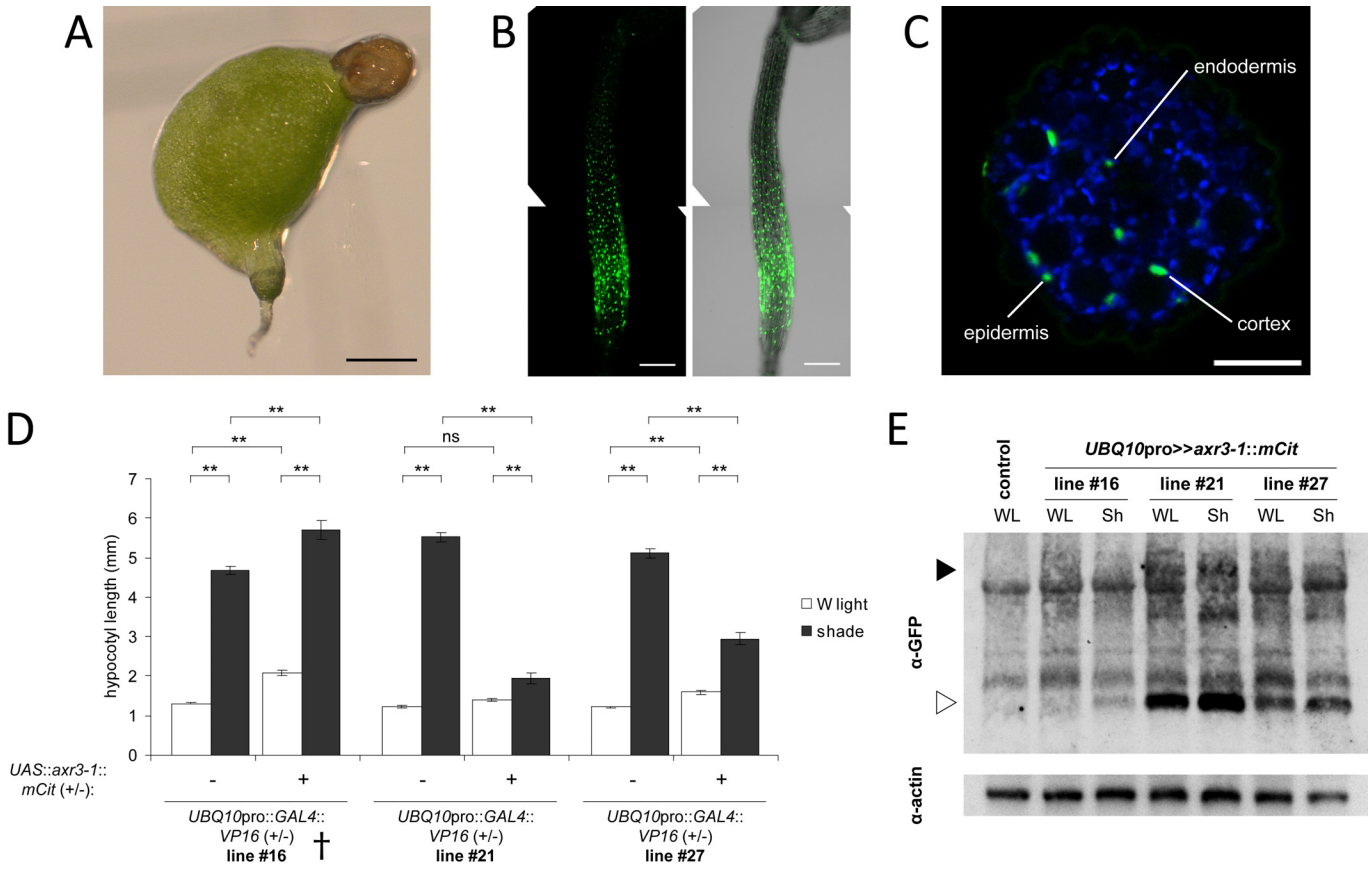

SUPPLEMENTAL FIGURE S1

Supplemental Figure S1. Broad expression of *axr3-1*::*mCit* under the *UBQ10* promoter resulted in *Arabidopsis* plants with embryonic and post-embryonic defects. (*A*) All three *UBQ10*pro::*GAL4*::*VP16* lines examined produced a small percentage of F1 seedlings with severe developmental defects when crossed to *UAS*::*axr3-1*::*mCit* plants. These defects included additional or missing cotyledons, and a lack of basal structures. An example of a 9 d-old W light-grown *UBQ10*pro>>*axr3-1*::*mCit* seedling with only a single cotyledon and lacking root and hypocotyl structures is pictured (line #16; for this line, 14% of seedlings lacked basal structures; *n* = 99). Scale bar, 500 µm. (*B*) Fluorescence image showing an example of axr3-1::mCit protein localization (green) in a 5 d-old W light-grown *UBQ10*pro>>*axr3-1*::*mCit* seedling. In our hands, expression of *UBQ*pro>>*axr3-1*::*mCit* was affected by organ type and developmental stage, with strongest expression in the root. In the hypocotyl, axr3-1::mCit expression was inconsistent, and sometimes stronger in either the base or the apex. We did not detect visible axr3-1::mCit fluorescence in the hypocotyl of 9 d-old seedlings, although expression in the roots was still strong (data not shown). Scale bar, 200 µm. (*C*) Cross-section through the hypocotyl of a 5 d-old W light-grown *UBQ*pro>>*axr3-1*::*mCit* seedling. Chlorophyll autofluorescence (blue) shows the position of the cortical cells, while examples of nuclear-localized axr3-1::mCit protein (green) are indicated. Scale bar, 50 µm. (*D*) Hypocotyl length of different, randomly selected *UBQ10*pro>>*axr3-1*::*mCit* lines treated with W light or shade. Only seedlings that developed a hypocotyl and root were scored. Seedlings are hemizygous (+/-) for the indicated transgenes. Data show mean +/- SEM. Tukey's HSD calculated within each line, $^{**}p < 0.005$, ns = not significant. It is not clear to us why line #16 shows an opposite phenotype to the other two lines (†), but might reflect differences in spatial and developmental regulation of the *axr3-1*::*mCit* sequence in this line, or be a consequence of lower levels of axr3-1::mCit protein (see panel *E*), which might alter the interplay between blocking auxin responses with feedback on auxin production. (*E*) Western blot against axr3-1::mCit (recognized by α-GFP) using protein extracted from the different *UBQ10*pro>>*axr3-1*::*mCit* lines. Protein was extracted from 9 d-old W light (WL)- and shade (Sh)-treated plants. Control genotype is plants hemizygous for the *UAS*::*axr3-1*::*mCit* transgene only. Solid arrowhead indicates the position of where full-length axr3-1::mCit protein is expected to run, while the open arrowhead indicates the expected position of free mCit. Note that relatively high levels of axr3-1::mCit protein degradation were observed in these lines (by contrast, compare to other cell-specific pro>>*axr3-1*::*mCit* lines shown in Supplemental Fig. S3). (*F-G*) Examples of 9 d-old *UBQ10*pro>>*axr3-1*::*mCit* line #21 and #27 seedlings grown as in *D*. Note the range of phenotypes, including root and hypocotyl agravitropism, single cotyledons, and multiple roots stemming from the hypocotyl-root junction. Scale bars, 5 mm. Data for the *UBQ10*pro>>*axr3-1*::*mCit* line with the strongest expression (line #21) is shown in Fig. 1A of the main paper.

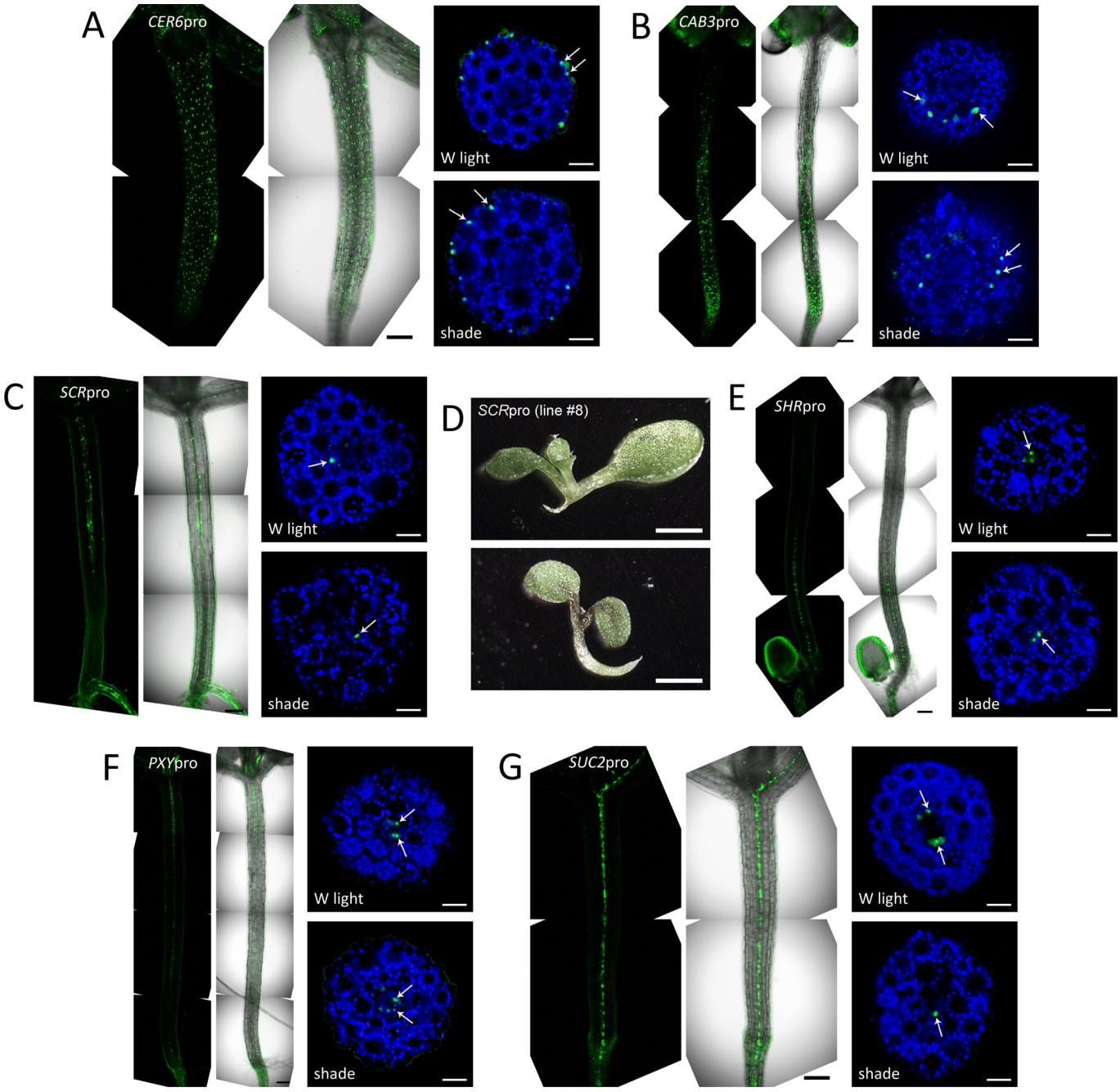

Supplemental Figure S2. Expression analysis of different cell-specific pro>>*axr3-1*::*mCit Arabidopsis* plants. (*A*-*C* and *E*-*G*) Representative fluorescence images of cell-specific pro>>*axr3-1*::*mCit* plants. axr3-1::mCit protein localization (green) along the hypocotyl of 9 d-old W light-grown plants is shown at left. At right, W light- and shade-treated 9 d-old hypocotyl cross-sections are shown. Images are from plants expressing *axr3-1*::*mCit* under *CER6*pro (*A*), *CAB3*pro (*B*), *SCR*pro (*C*), *SHR*pro (*E*), *PXY*pro (*F*) and *SUC2*pro (*G*). Chlorophyll autofluorescence (blue) in cross-sections shows the position of the cortical cells, while arrows indicate examples of nuclear-localized axr3-1::mCit protein. *SCR*pro drives expression mostly in the upper hypocotyl, while *SHR*pro mostly in the lower. Note that cell-specific protein localization in hypocotyl cross-sections does not change between W light and shade treatments. Scale bars are 200 µm for hypocotyl longitudinal views, and 50 µm for cross-sections. (*D*) One of three *SCR*pro>> *axr3-1*::*mCit* lines tested (line #8) produced seedlings with embryonic defects at a high frequency (80% of seedlings lacked either the root, or the root and hypocotyl; *n* = 88). Examples of 9 d-old seedlings lacking basal structures are shown. Scale bar, 1 mm.

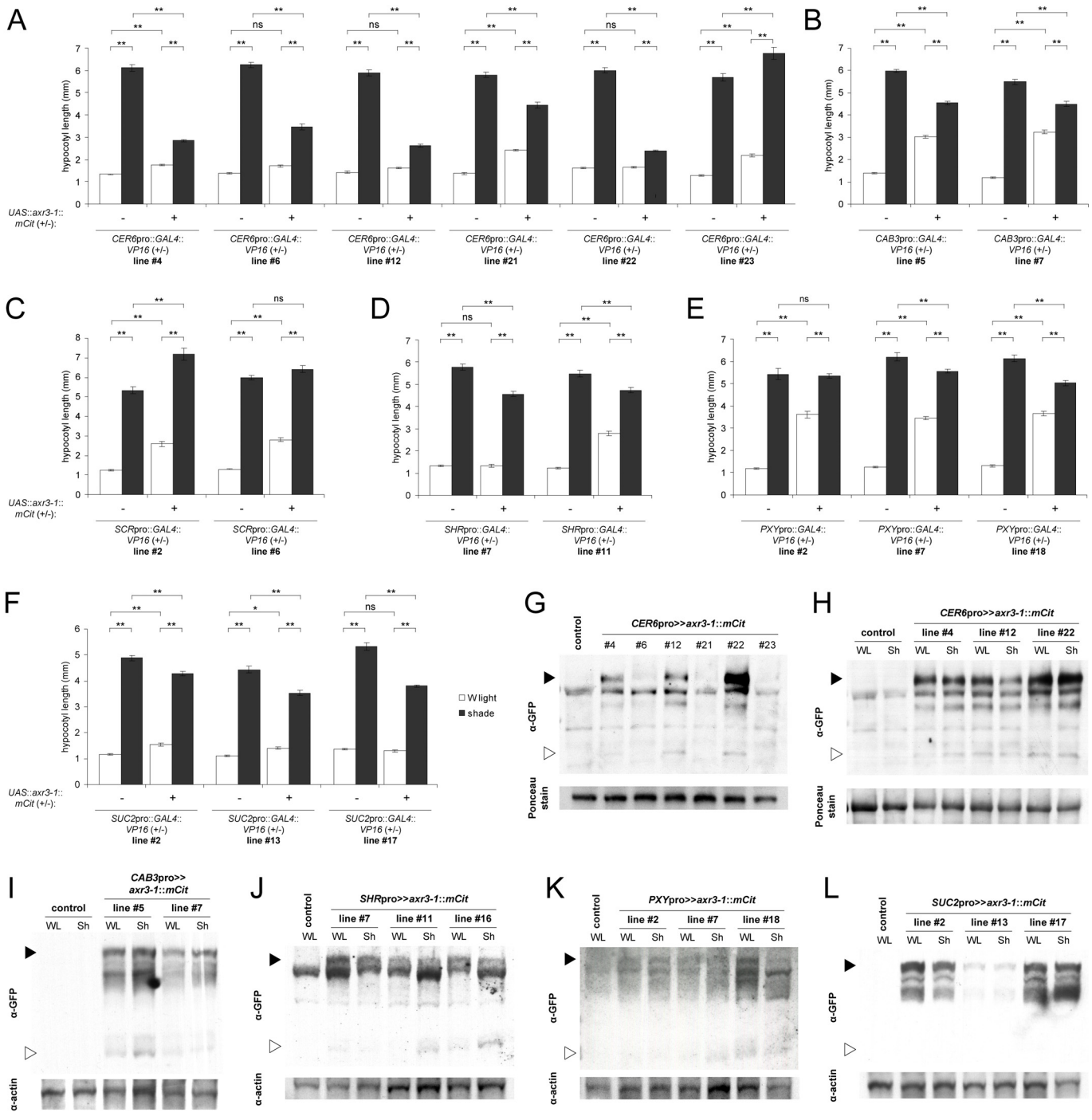

SUPPLEMENTAL FIGURE S3

Supplemental Figure S3. Hypocotyl growth defects of cell-specific pro>>*axr3-1*::*mCit* lines correlates with axr3-1::mCit protein level. (*A*-*F*) Hypocotyl length of different cell-specific pro>>*axr3-1*::*mCit* lines following W light or shade treatment. Plants are hemizygous (+/-) for the indicated transgenes. Experimental plants (hemizygous for both *UAS*::*axr3-1*::*mCit* and cell-specific pro::*GAL4*::*VP16*) are compared to control plants hemizygous for only the cell-specific pro::*GAL4*::*VP16* transgene for each line. Cell-specific promoters used are *CER6*pro (*A*), *CAB3*pro (*B*), *SCR*pro (*C*), *SHR*pro (*D*), *PXY*pro (*E*) and *SUC2*pro (*F*). Hypocotyl length was not scored for an additional *SCR*pro line (#8), which had a high incidence of developmental abnormalities. Similarly, an additional *SHR*pro line (#16) did not germinate well and had defective growth, and was not scored. Data show mean hypocotyl length +/- SEM. Tukey's HSD calculated within each line, $^{**}p < 0.005$, $^{*}p < 0.05$, ns = not significant. Data for the following cell-specific pro>>*axr3-1*::*mCit* lines is replicated in Fig. 2G of the main paper: *CER6*pro, #22; *CAB3*pro, #7; *SCR*pro, #6; *SHR*pro, #11; *PXY*pro, #18; and *SUC2*pro, #17 (generally, the line with the strongest effect on hypocotyl growth). (*G*-*L*) Western blots against axr3-1::mCit (recognized by α-GFP) using protein extracted from the different cell-specific pro>>*axr3-1*::*mCit* lines. Protein was extracted from 9 d-old W light (WL)- and shade (Sh)-treated plants. Cell-specific promoters are *CER6*pro (*G*, WL-grown only; and *H*, WL and Sh), *CAB3*pro (*I*), *SHR*pro (*J*), *PXY*pro (*K*) and *SUC2*pro (*L*). Control genotype is plants hemizygous for the *UAS*::*axr3-1*::*mCit* transgene only. We could not detect protein expression using standard western blotting techniques for the *SCR*pro>>*axr3-1*::*mCit* lines. Solid arrowheads indicate the position of where the full-length axr3-1::mCit protein is expected to run, while the open arrowheads indicate the expected position of free mCit.

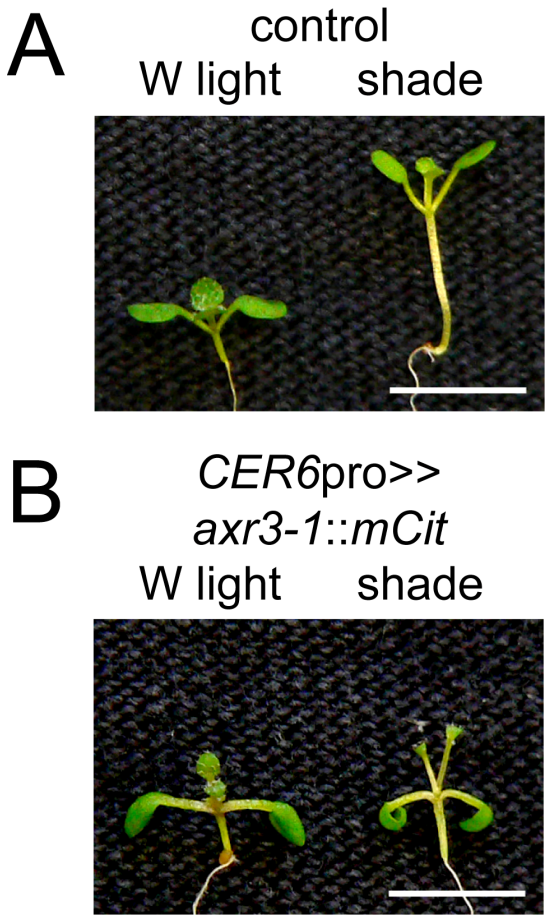

Supplemental Figure S4. Blocking transcriptional responses to auxin in the epidermis alters hypocotyl growth. (*A-B*) Representative images of W light- and shade-treated control (*A*) and *CER6*pro*>>axr3-1*::*mCit Arabidopsis* seedlings (*B*). Scale bars, 5 mm. Control is hemizygous for the *UAS*::*axr3-1*::*mCit* transgene.

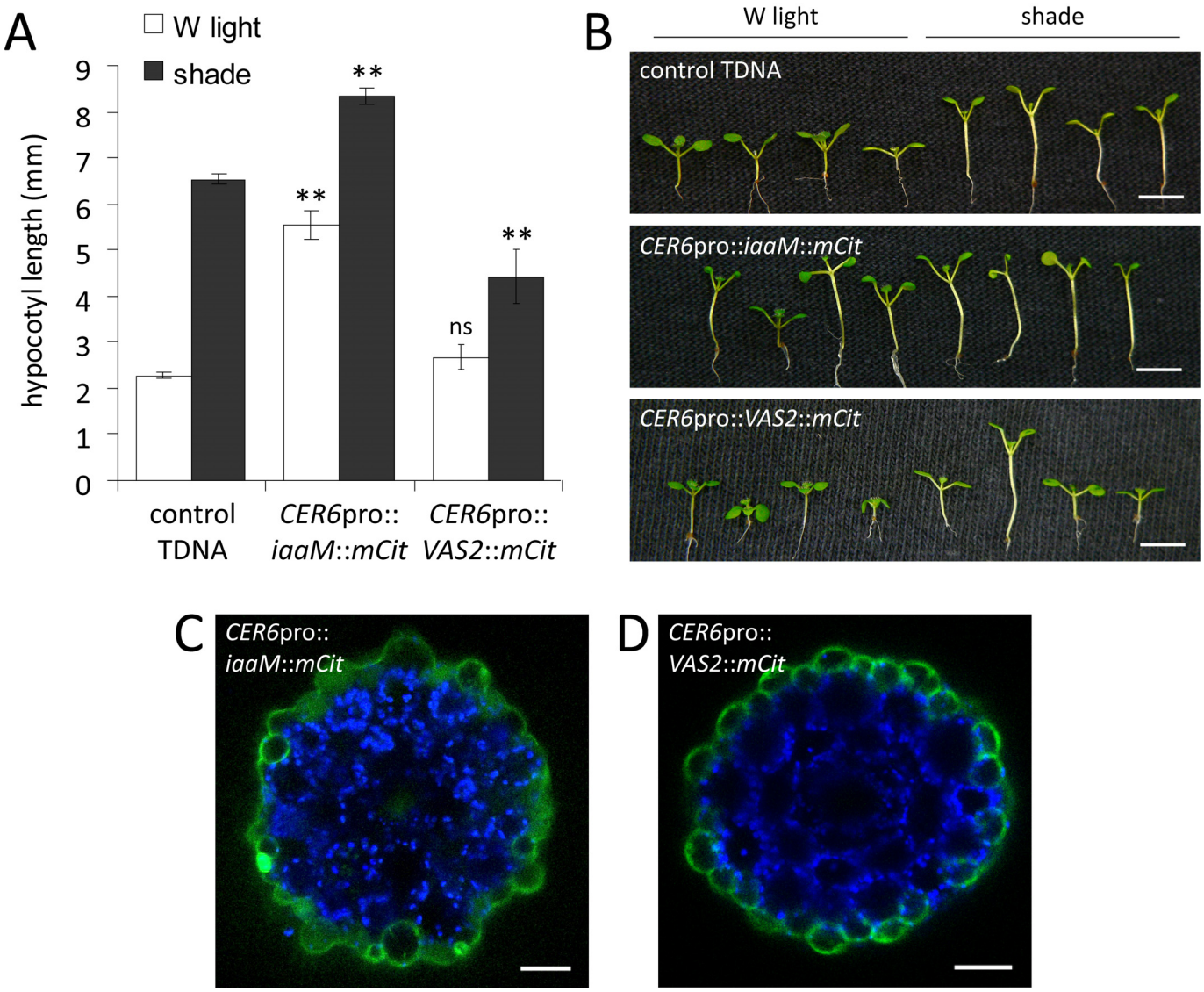

Supplemental Figure S5. Auxin synthesis or inactivation in the epidermis alters hypocotyl length. (*A*) Hypocotyl length of 9 d-old *Arabidopsis* seedlings expressing *iaaM*::*mCit* or *VAS2*::*mCit* under the control of *CER6*pro. First generation transgenic (T1) seedlings were scored on kanamycin selection medium (50 µg/mL). The control TDNA used is *IAA17*pro::*GUS*::*mCit*, which also carries kanamycin resistance. Data show mean +/- SEM. Means are compared to the control TDNA grown in the same light condition using Tukey's HSD, $^{**}p < 0.005$, ns = not significant. Note that the hypocotyls of iaaM expressing plants are longer in both W light and shade, most likely due to increased auxin production in both light conditions. (*B*) Representative images of W light- and shade-treated T1 seedlings grown as in *A*. Because of variation in kanamycin resistance and transgene expression, variations in the phenotype are observed. Scale bars, 5 mm. (*C*-*D*) Hypocotyl cross-sections showing iaaM::mCit (C) and VAS2::mCit (D) protein localization (green) in 9 d-old T1 seedlings expressing the protein from *CER6*pro. Chlorophyll autofluorescence (blue) shows the position of the cortical cells. Note iaaM::mCit and VAS2::mCit localization to the epidermis. Scale bars, 50 µm.

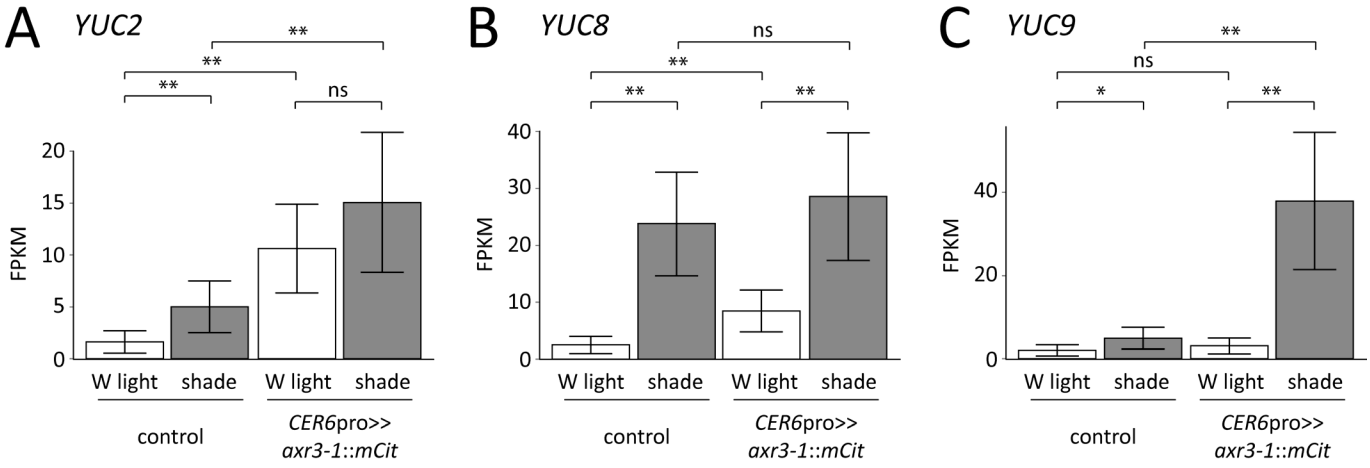

Supplemental Figure S6. Auxin responses in the epidermis feed back onto auxin production. (*A*-*C*) Gene expression values as measured by RNA-Seq for *YUC2* (*A*), *YUC8* (*B*) and *YUC9* (*C*) genes, for plants treated as in Fig. 3 of the main paper. Error bars represent confidence intervals. False discovery rate, ** $q < 0.005$, * $q < 0.05$, ns = not significant. Data was visualized using cummeRbund (Goff et al. 2013).

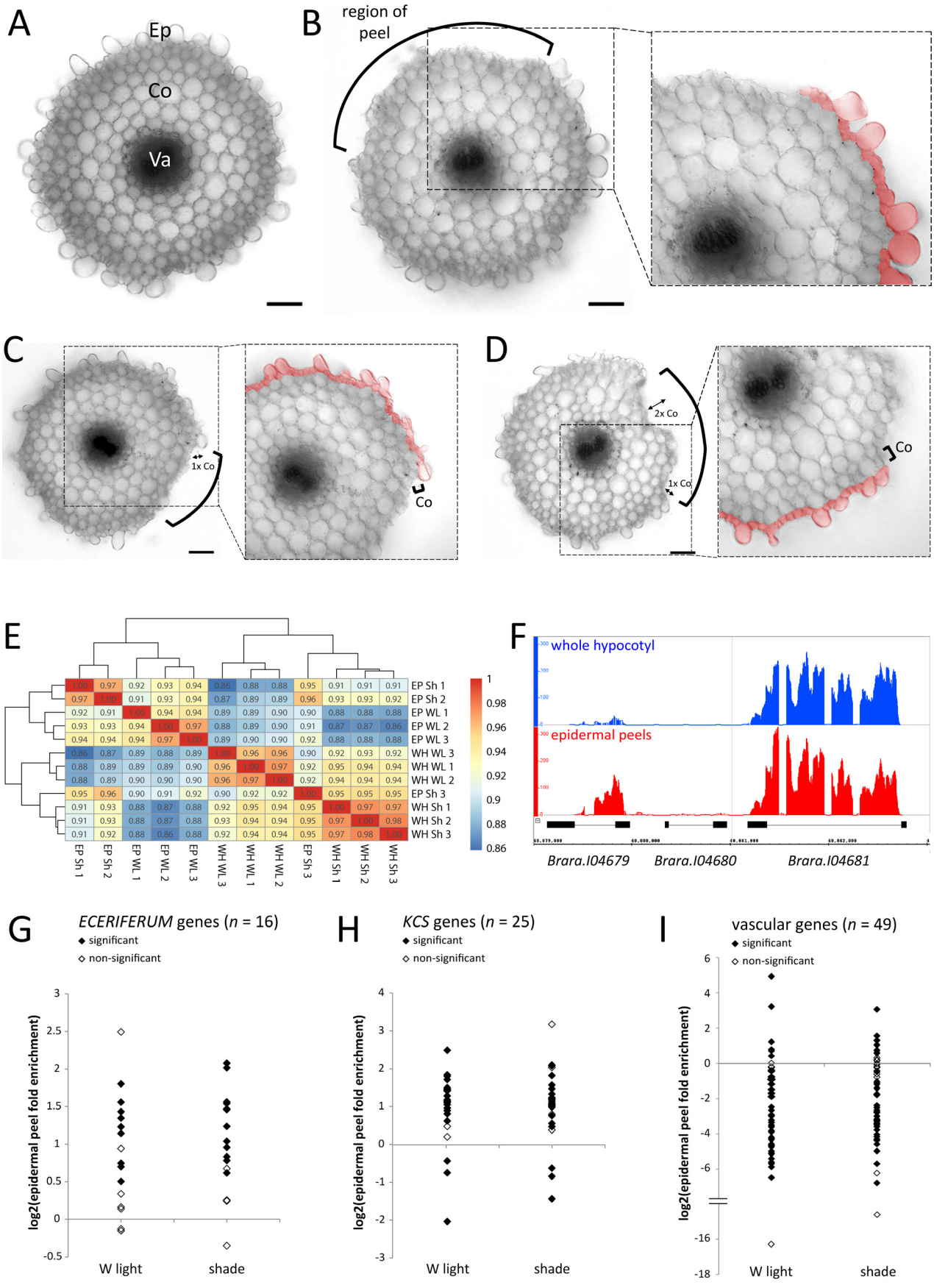

SUPPLEMENTAL FIGURE S7

Supplemental Figure S7. Epidermal peels from *Brassica rapa* hypocotyls can successfully enrich for epidermis-specific gene expression. (*A*) Light microscopy image of a cross-section through a 4 d + 9 h W light-grown *Brassica* hypocotyl. Note the additional layers of cortex compared to *Arabidopsis*. Ep, epidermis; Co, cortex; Va, vasculature. (*B*) Cross-section along the flank of the hypocotyl after an epidermal peel has been removed. Boxed region is magnified on right, and epidermal cells are shaded red. Note that our method removes the single outermost layer of epidermal cells along the hypocotyl flank. (*C*,*D*) Examples of cross-sections at the very top or bottom of the hypocotyl where forceps were used to grip the outer cell layers and begin the epidermal peel. Note that at these positions, one or two layers of cortical cells are also removed with the epidermis. In *A*-*D*, scale bars, 100 µm. (*E*) Correlations between gene expression profiles of *B. rapa* whole hypocotyl (WH) and hypocotyl epidermal peel (EP) samples. 4 d-old W light-grown seedlings were treated with either 9 h W light (WL) or shade (Sh) prior to tissue collection. Each sample type was collected in biological triplicate, and gene expression measured by RNA-Seq. Spearman correlation coefficients are shown using the expression values for all genes. Note that epidermal peel expression profiles are generally more similar to one another than they are to whole hypocotyl tissue, regardless of light treatment. When we compared replicates, we noticed that one of our shade-treated epidermal peel samples (EP Sh 3) was more similar to shade-treated whole hypocotyl tissue, suggesting that this sample was contaminated with an unacceptable number of cells from the inner tissues. This sample was subsequently discarded from all further analyses. (*F*) Screenshot from the Integrated Genome Browser (Nicol et al. 2009) showing a summed depth chart of RNA sequencing alignments against the *B. rapa* genome. Top, summed read alignments for the three whole hypocotyl tissue replicates collected from W light-treated seedlings (blue), and below, for epidermal peel replicates (red). The region spans three genes, indicated at bottom. Note increased expression of *Brara.I04679* in the epidermal peels, which codes for a putative ortholog of *EPIDERMAL PATTERNING FACTOR1* (*EPF1*). In *Arabidopsis*, *EPF1* is expressed in immature guard cells and epidermal cells destined to become stomata (Hara et al. 2007). (*G*-*I*) Fold-enrichment of gene expression values from epidermal peels compared to whole hypocotyl tissue in W light- and shade-treated seedlings. Shown are putative orthologs of *ECERIFERUM* genes from *Arabidopsis* (*G*), 3-ketoacyl-CoA synthase (KCS) gene family members (*H*), and vascular genes (*I*; vascular genes were previously identified as differentially expressed in xylem and cambium/phloem by microarray analysis (Zhao et al. 2005)). *eceriferum* (*cer*) mutants in *Arabidopsis* have defects in epicuticular wax deposition (Koornneef et al. 1989), and one of these genes, *CER6*, codes for a member of the 3-ketoacyl-CoA synthase (KCS) gene family, required for fatty acid elongation. Transcriptional reporters for *CER6* and some other *KCS* genes are expressed in the *Arabidopsis* epidermis, suggesting that many members of this family have roles in cuticular wax production in the epidermis (Joubes et al. 2008). We find that expression of *ECERIFERUM* and *KCS* putative orthologs are more likely to be enriched in the epidermal peels than not, and vice versa for the vascular-associated genes ($p < 0.005$, one-sided Fisher's exact tests). Only those genes with FPKM > 0 in all tissue samples are shown (reflected in *n* values). Filled diamonds indicate expression values in epidermal peels that are significantly different from whole hypocotyl tissue (false discovery rate, $q < 0.05$).

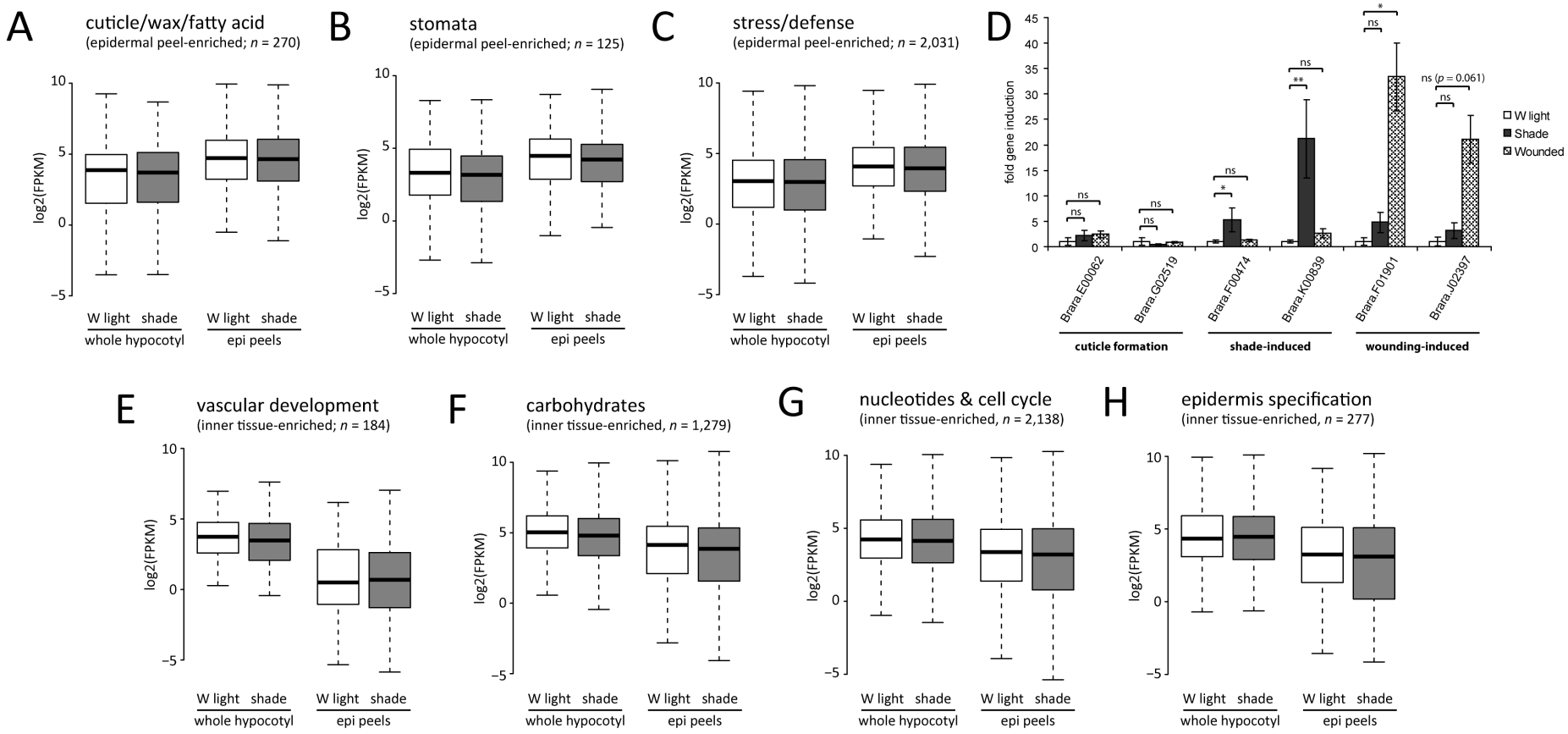

SUPPLEMENTAL FIGURE S8

Supplemental Figure S8. The *B. rapa* hypocotyl epidermis and inner tissues are enriched for expression of genes with different biological functions. (*A*,*B*) We performed GO term enrichment analysis by assigning each *Brassica* gene the same GO terms as its putative ortholog from *Arabidopsis*, on the assumption that these genes would serve a similar function in the two species. We found that GO terms related to epidermal cuticle formation and stomata function were enriched amongst the genes more highly expressed in the epidermal peels (see Supplemental Table S9). Box plots showing expression values of the epidermal peel-enriched genes associated with these GO terms are shown. (*C*) As in *A*,*B*, except for genes associated with GO terms related to stress and defense. We used a relaxed criteria for this category, and included GO terms related to environmental stress responses (e.g. response to insects, drought, wounding, fungus, etc) and also terms related to hormonal pathways involved in these responses, including jasmonic acid, salicylic acid and ethylene (see Supplemental Table S9). The expression of some of these genes might reflect the role the epidermis and cuticle serve in protecting the plant from environmental stressors (Kunst and Samuels 2003), or represent a wounding response elicited during the peeling process (see panel *D*). (*D*) Expression analysis of *Brassica* whole hypocotyl tissue by quantitative reverse transcriptase PCR (qRT-PCR). In our RNA-Seq experiment, epidermal peels were left at incubator temperature anywhere from 0-15 min before snap freezing in liquid N_2 and RNA extraction. To test if this time frame was sufficient for wounding response genes to be activated, we employed a qRT-PCR approach. We found that two putative orthologs of genes associated with the GO term "response to wounding" (*Brara.F01901* and *Brara.J02397*) were induced within 15 min in mechanically-damaged whole hypocotyl tissue by qRT-PCR. *Brassica* seedlings were grown for 4 d + 9 h in W light, hypocotyls were removed, dissected into pieces and ground with a micropestle. Damaged tissue was left for 15 min before snap freezing in liquid N_2. Damaged tissue (Wounded) was compared to undamaged hypocotyl tissue that was immediately snap frozen after dissecting from whole seedlings (W light). By contrast, putative orthologs for two genes involved in cuticle formation and which also had enriched expression in our epidermal peels (*Brara.E00062* and *Brara.G02519*) did not significantly change in response to wounding. Similarly, genes found in our RNA-Seq experiment to be highly shade-induced (*Brara.F00474* and *Brara.K00839*, of which, notably, *Brara.F00474* codes for a 3-ketoacyl-CoA synthase homologue also highly enriched in the epidermal peels) were not affected by physical wounding but were induced by shade as assessed by qRT-PCR (4 d-old W light-grown seedlings treated with 9 h shade [Shade]). Small but significant changes in gene expression that we detected by RNA-Seq were unable to be detected by our qRT-PCR methods. Due to a recent genome triplication event in *B. rapa* (Wang et al. 2011), our qRT-PCR primers may recognize paralogous genes with similar affinity (see Supplemental Methods). In summary, these results suggest that the activation of wounding response genes in our epidermal peels is likely an artifact of the peeling process, but that it is unlikely that wounding affects the expression of shade-induced and other epidermis-enriched genes. Data show mean fold-induction for each gene over the respective W light control, +/- SEM. Student's t test, $**p < 0.005$, $*p < 0.05$, ns = not significant. (*E*-*G*) GO terms associated with inner tissue-enriched genes included terms related to vascular development, carbohydrate metabolism, and cell cycle (including nucleotide synthesis and DNA replication; see Supplemental Table S10). Box plots showing expression values of genes significantly enriched in the inner tissues that are associated with these GO terms are shown. Carbohydrate metabolism may reflect function of the inner photosynthetic cortical cells, while the high number of cell cycle-related genes suggests that the inner tissue has at least one actively dividing cell population. This might be dividing vascular cells undertaking secondary thickening of the hypocotyl stem (Lehmann and Hardtke 2016). By contrast, in the post-embryonic Arabidopsis hypocotyl, epidermal cells elongate but do not divide, although endoreduplication is present (Gendreau et al. 1997). It is likely that epidermal cells of the Brassica hypocotyl also divide little during shade-induced growth (Procko et al. 2014). (*H*) Interestingly, we also noticed terms associated with epidermis specification being enriched amongst the inner tissue genes (see Supplemental Table S10). This might reflect limitations in the previously assigned GO terms, or indicate that genes expressed in the inner layers can affect epidermal fate non-cell autonomously. A box plot for the genes associated with these GO terms and which also have enriched expression in the inner tissues is shown.

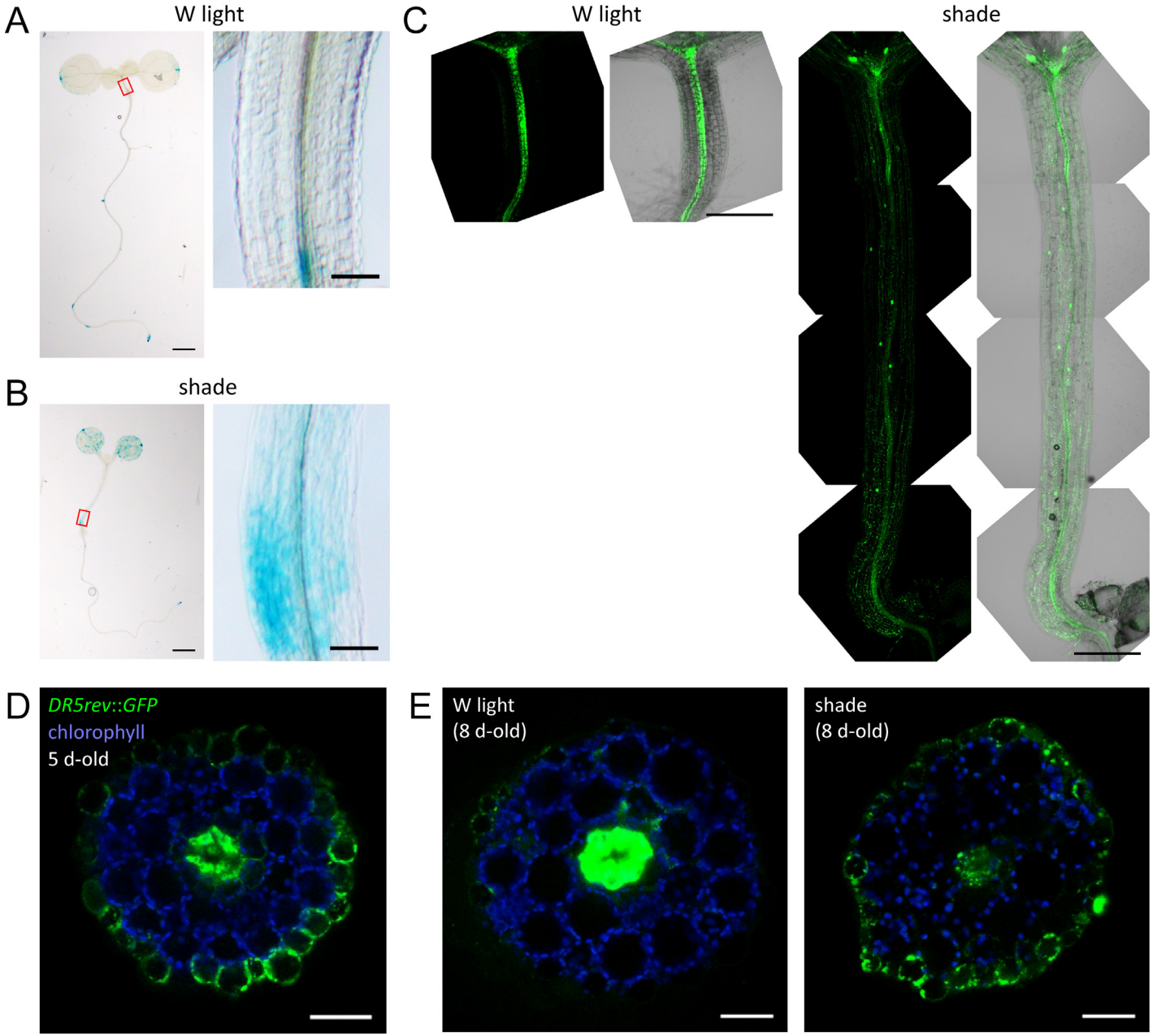

SUPPLEMENTAL FIGURE S9

Supplemental Figure S9. The *DR5* auxin reporter shows a redistribution of activity from the vasculature to the outer layers of the hypocotyl following shade perception in *Arabidopsis*. (*A*,*B*) Images of GUS-stained whole seedlings (left) and close-up of the hypocotyl (right) of *Arabidopsis* plants carrying a *DR5*::*GUS* reporter. Plants were grown either in W light for 8 d (*A*) or 5 d W light + 3 d shade (*B*). Red box on left marks the region magnified on right. Most hypocotyl staining is observed near the base. Note increased *DR5*::*GUS* reporter activity in the outer cell layers of shade-treated hypocotyls in addition to vascular staining. Scale bars represent 1 mm (left) and 0.1 mm (right). (*C*) Representative fluorescence images showing ER-localized GFP (green) driven by a *DR5rev*::*GFP* reporter (Benkova et al. 2003) along the hypocotyl of *Arabidopsis* seedlings grown in 9 d W light (left) or 5 d W light + 4 d shade (right). Scale bars, 500 µm. (*D*,*E*) Fluorescence images of *DR5rev*::*GFP* activity in hypocotyl cross-sections of 5 d-old W light-grown seedlings (*D*), or plants treated as in *A*,*B* (*E*). Chlorophyll autofluorescence (blue) shows the position of the cortical cells. Scale bars, 50 µm. Within panels *C*,*E*, exposure of GFP is kept constant. Note relative redistribution of GFP from the vasculature to the epidermis and outer layers of shade-treated plants in *C*,*E*.

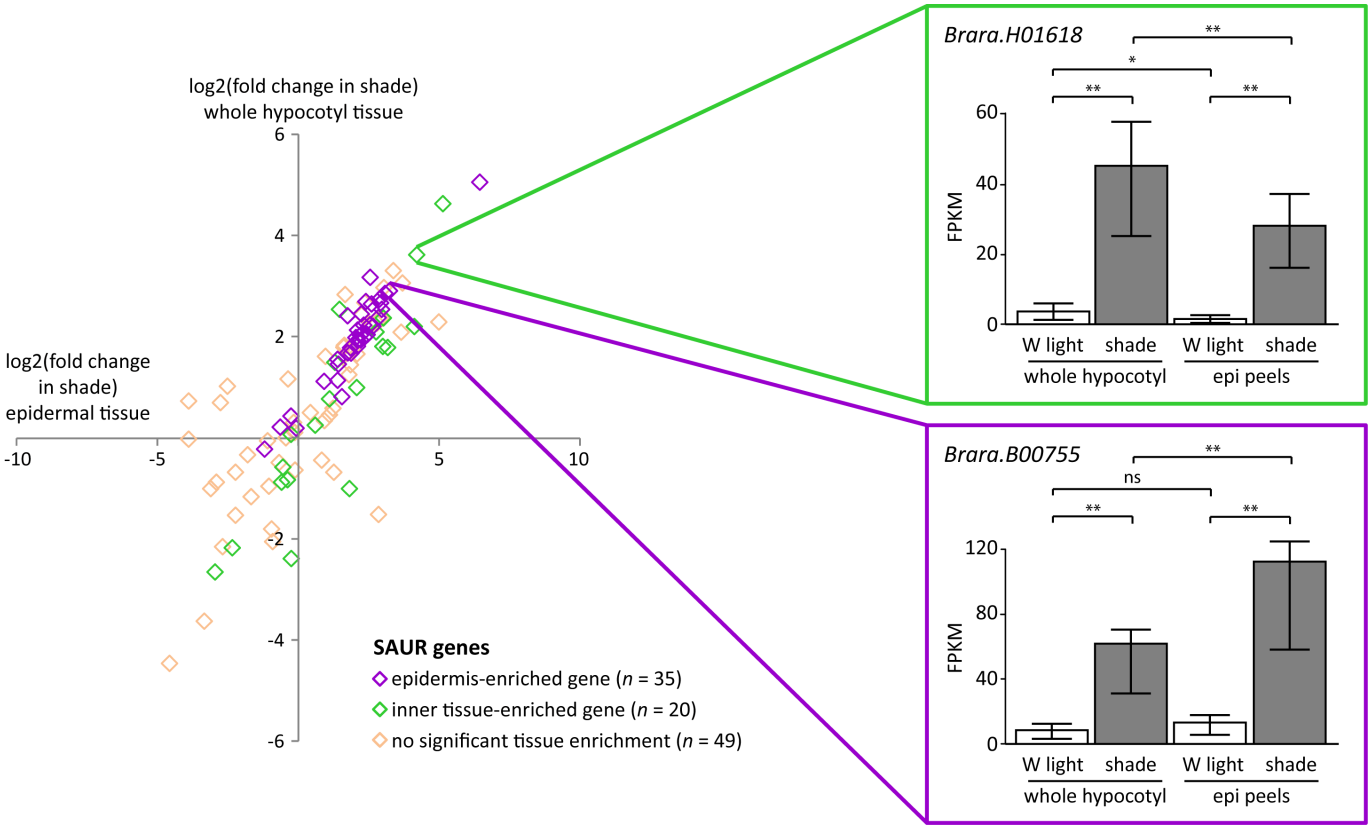

Supplemental Figure S10. The epidermis and inner tissues have distinct responses to shade. Left, fold change of gene expression in response to shade for all *B. rapa SAUR* genes with FPKM > 0 in all samples (see Fig. 6H of the main paper). Right, examples of *SAUR* genes with enriched expression in the inner tissues (top) or the epidermis (below), which are induced by shade. Error bars represent confidence intervals. False discovery rate, $^{**}q < 0.005$, $^{*}q < 0.05$, ns = not significant.

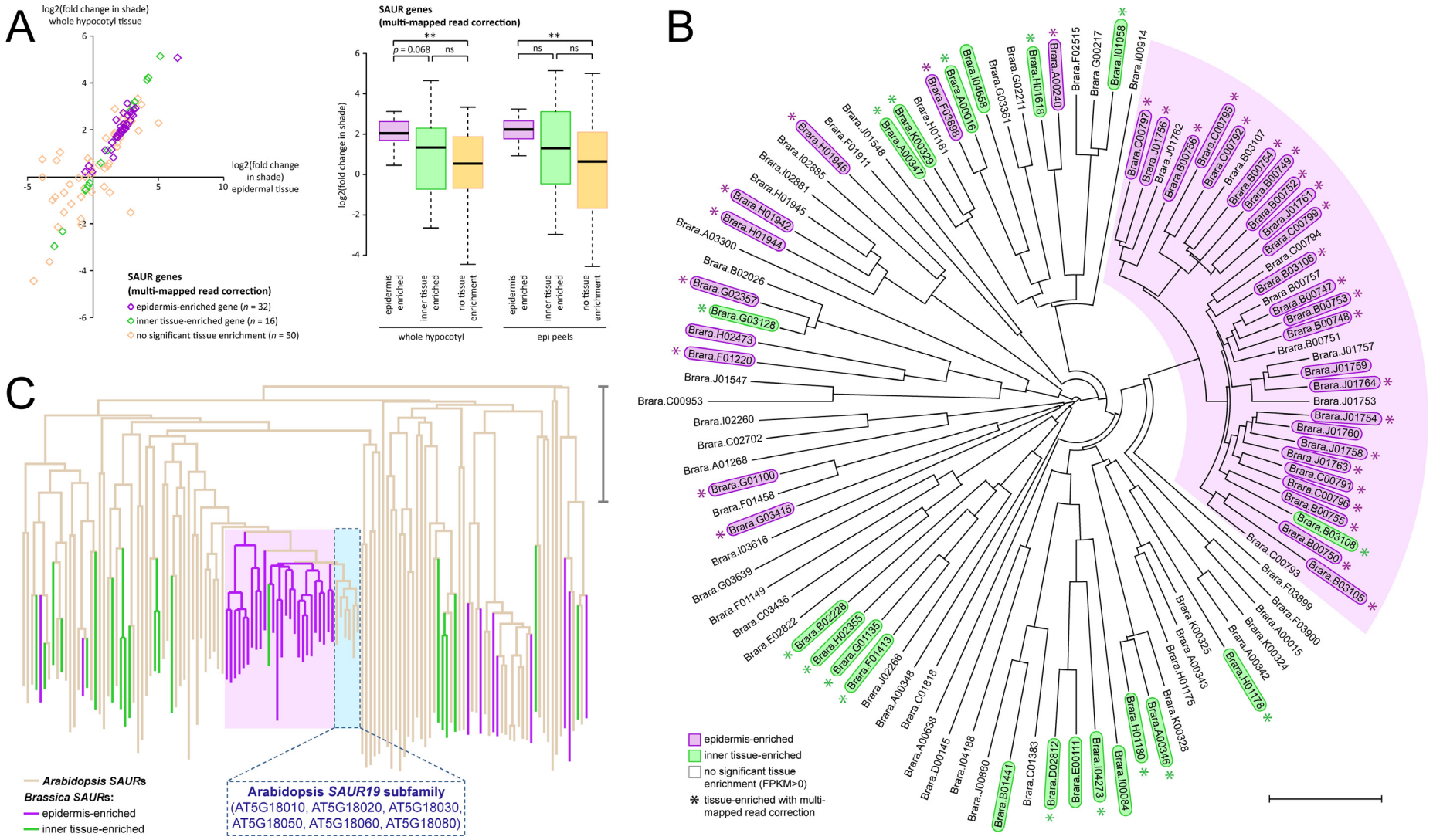

SUPPLEMENTAL FIGURE S11

Supplemental Figure S11. A *SAUR* gene subfamily has enriched expression in the *B. rapa* hypocotyl epidermis. (*A*) Re-analysis of our *Brassica* RNA-Seq data of *SAUR* gene family members using multi-mapped read correction. Left, fold change in shade of gene expression in whole hypocotyl tissue (*y* axis) plotted against fold change in epidermal peel samples (*x* axis). Genes that are significantly enriched in either the epidermis or inner tissues (in either W light or shade), or that have no significant tissue enrichment are indicated. Only SAUR genes with FPKM > 0 in all tissue samples are shown. Right, box plot of these same *SAUR* genes. Tukey's HSD, $^{**}p < 0.005$, ns = not significant. Note that these results are similar to those obtained using our default analysis method without multi-mapped read correction (Fig. 6G,H of the main paper). (*B*) A possible phylogenetic tree of *Brassica SAUR* family genes, based on coding sequence alignment using the MUSCLE algorithm (default settings) and Dendroscope v3.5.7 tree viewing software, with midpoint rooting (Edgar 2004; Huson and Scornavacca 2012). Only *SAUR* family genes with FPKM > 0 in all tissue samples in our RNA-Seq data are shown. Boxed genes represent those with significant enrichment in either the epidermis or inner tissues using our default analysis method. Asterisks indicate those with significant enrichment using multi-mapped read correction. Note that most of the epidermis-enriched *SAUR* genes are within the same clade (shaded purple). (*C*) A possible phylogenetic tree comparing the *Brassica SAUR* family genes with tissue enriched expression against all 79 *Arabidopsis SAUR*s. Note that the *Arabidopsis SAUR19* subfamily falls within the epidermis-enriched clade identified in *B*. In *B*,*C*, scale bars, 0.1 nucleotide substitutions per site.

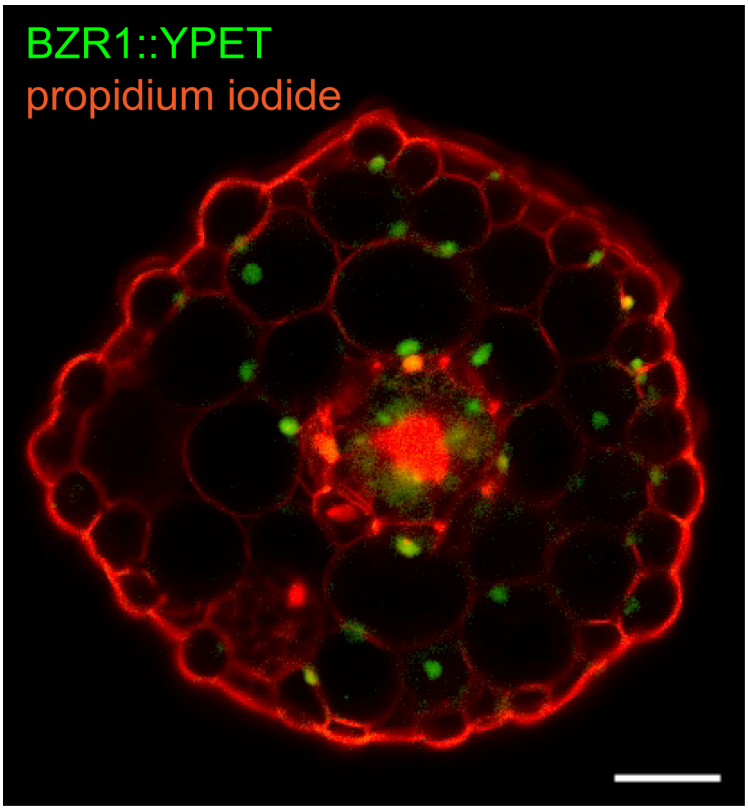

Supplemental Figure S12. *BZR1*::*YPET* is expressed in most cells of the hypocotyl. Fluorescence image of a hypocotyl cross-section of a 9 d-old *Arabidopsis* seedling expressing *BZR1*::*YPET* (green), and counterstained with propidium iodide (red). Note nuclear BZR1::YPET protein localization in most, if not all cell types. Scale bar, 50 µm.

Supplemental materials and methods

DNA constructs and plant transformation

The multisite Gateway system (Invitrogen) was used for all constructs, except the *BZR1*::2x*YPET*::3x*HA* recombineered BAC clone. 2 kb *CER6*pro, 1.5 kb *CAB3*pro, 2 kb *PXY*pro, 3.5 kb *SUC2*pro, 2 kb *IAA17*pro, and 2.4 kb *SAUR19*pro were PCR amplified from Col-0 genomic DNA and recombined into pDONR-P4P1R, except *SAUR19*pro which was cloned into pDONR221. The *UBQ10*pro, *SCR*pro and *SHR*pro in pDONR-P4P1R were as previously described (Jaillais et al. 2011; Marques-Bueno et al. 2016). The *UAS* regulatory sequence (5x *UAS* with -46 CaMV minimal promoter) was amplified from an *Arabidopsis* GAL4 enhancer trap line (Haseloff 1999) and recombined with pDONR-P4P1R. *GUS*, *axr3-1* (amplified from cDNA generated from *axr3-1* mutants), *iaaM*, *VAS2*, and *GAL4*::*VP16* (amplified from an *Arabidopsis* GAL4 enhancer trap line) cDNA fragments were recombined into pDONR221. To generate cell specific pro::*GAL4*::*VP16* constructs, the promoter and *GAL4*::*VP16* sequences were recombined into the destination vector pK7m34GW with a pDONR-P2RP3 plasmid carrying a 25 bp random sequence. To generate *IAA17*pro::*GUS*::*mCit* and *CER6*pro::*iaaM*/*VAS2*::*mCit* constructs, the promoter and cDNA fragments were recombined with the *mCit* sequence in pDONR-P2RP3 into pK7m34GW. The *mCit* vector was previously described (Jaillais et al. 2011). *UAS*, *axr3-1* and *mCit* sequences were recombined into pB7m34GW to create *UAS*::*axr3-1*::*mCit*. To generate *SAUR19pro*::*GFP*::*GUS* constructs, the promoter was recombined into pBGWFS7. For all constructs, Col-0 were transformed with *Agrobacterium* GV3101 carrying the various constructs using standard techniques, and segregation analyses were used to isolate single-insertion homozygous lines.

The *BZR1*::*YPET* line was generated by BAC recombineering using BAC clone JAtY72J14 (length 74,256 bp). The recombineering method was as described previously (Warming et al. 2005). Primers used had 50 bp of homology to 5' and 3' sequences immediately flanking the *BZR1* stop codon. Briefly, the *BZR1* stop codon in the BAC was deleted and replaced with the *galK* gene using positive selection. The *galK* marker was then replaced with a 2x*YPET*::3x*HA* PCR product with flanking sequence homology using negative selection. Primers used for confirming and sequencing the insertion and fusion of 2x*YPET*::3x*HA* to the *BZR1* gene were ACTGCTGCCTTCCAAGAGATTG and AAGTGAAGAACATATGAGATTCCAT. Col-0 plants were transformed and YPET expression was assessed in the roots of basta-resistant transformants. Of 12 single insertion lines, 5 gave no signal, while 7 had similar expression patterns. The line with the brightest root signal (#9) was chosen for hypocotyl imaging.

Four independent *IAA17*pro::*GUS*::*mCit* reporter lines were stained for GUS activity. One had weak to no staining, while three had similar staining patterns. Two of these stained in the mid-upper hypocotyl, while the other had weak and occasionally no hypocotyl staining. The line with the strongest expression (#16) is shown in Fig. 1.

Western blot analysis

Western blots and GUS staining were performed using standard protocols. Primary antibodies used were α-GFP (Roche) and α-actin (MP Biomedicals).

qRT-PCR of Brassica samples

qRT-PCR was performed using standard techniques, using 3 biological replicates. Fold changes in gene expression were calculated using the ΔΔCt method. Previously, we reported qRT-PCR primers for shade-induced marker genes in *Brassica* using a candidate approach (Procko et al. 2014). Here, we used our RNA-Seq results to design improved primers to a reference gene, and shade and wounding-response genes. Primers were: *Brara.K01792* (reference gene; GTCGTCTTCTCAAATCTCCCTC and TAACCTTGCCACAGATTCGT), *Brara.E00062* (TTCCAAACCCTGAAGTCGTG and ATGATGTGTTCTTGCAACTCC), *Brara.G02519* (CATTACATTCCTCCGACACCA and CCATAGCCGTGAAGATAACCA), *Brara.F00474* (CATTGTTAGTTCAGGTATCGGAG and GAGCGTCTTGTATGGTAGGAG), *Brara.K00839* (CAATCTGTTGCTGTGTATGCT and ATCTCTGTCACGAACCTTTCC), *Brara.F01901* (GACGACGATCATCAATTCGG and TCCGCTGATTAGCTCAAACTC), and *Brara.J02397* (GCAGATGAGAAACCGAGGAC and CGAATCATTCTGGTAAGTGGAG). Because the *B. rapa* genome has undergone a recent genome triplication event (Wang et al. 2011), it is difficult to design effective primers specific for the gene of interest, and it is possible that our primers also report the expression of paralagous genes with high sequence identity (e.g. the primers against *Brara.G02519* will likely also target *Brara.B01798*, with one and two base mismatches in primer annealing). This limitation was even more apparent in our previously published primer sets; e.g. see Supplemental Table S4 and notes therein.

References for Supplemental Material

Benkova E, Michniewicz M, Sauer M, Teichmann T, Seifertova D, Jurgens G, and Friml J. 2003. Local, efflux-dependent auxin gradients as a common module for plant organ formation. *Cell* **115**(5): 591-602.

Edgar RC. 2004. MUSCLE: multiple sequence alignment with high accuracy and high throughput. *Nucleic Acids Res* **32**(5): 1792-1797.

Gendreau E, Traas J, Desnos T, Grandjean O, Caboche M, and Hofte H. 1997. Cellular basis of hypocotyl growth in Arabidopsis thaliana. *Plant Physiol* **114**(1): 295-305.

Goff L, Trapnell C, and Kelley D. 2013. cummeRbund: Analysis, exploration, manipulation, and visualization of Cufflinks high-throughput sequencing data. R package version 2.12.0.

Hara K, Kajita R, Torii KU, Bergmann DC, and Kakimoto T. 2007. The secretory peptide gene EPF1 enforces the stomatal one-cell-spacing rule. *Genes Dev* **21**(14): 1720-1725.

Haseloff J. 1999. GFP variants for multispectral imaging of living cells. *Methods Cell Biol* **58**: 139-151.

Huson DH and Scornavacca C. 2012. Dendroscope 3: an interactive tool for rooted phylogenetic trees and networks. *Syst Biol* **61**(6): 1061-1067.

Jaillais Y, Hothorn M, Belkhadir Y, Dabi T, Nimchuk ZL, Meyerowitz EM, and Chory J. 2011. Tyrosine phosphorylation controls brassinosteroid receptor activation by triggering membrane release of its kinase inhibitor. *Genes Dev* **25**(3): 232-237.

Joubes J, Raffaele S, Bourdenx B, Garcia C, Laroche-Traineau J, Moreau P, Domergue F, and Lessire R. 2008. The VLCFA elongase gene family in Arabidopsis thaliana: phylogenetic analysis, 3D modelling and expression profiling. *Plant Mol Biol* **67**(5): 547-566.

Koornneef M, Hanhart CJ, and Thiel F. 1989. A Genetic and Phenotypic Description of Eceriferum (cer) Mutants in Arabidopsis thaliana. *J Hered* **80**(2): 118-122.

Kunst L and Samuels AL. 2003. Biosynthesis and secretion of plant cuticular wax. *Prog Lipid Res* **42**(1): 51-80.

Lehmann F and Hardtke CS. 2016. Secondary growth of the Arabidopsis hypocotyl-vascular development in dimensions. *Curr Opin Plant Biol* **29**: 9-15.

Marques-Bueno MM, Morao AK, Cayrel A, Platre MP, Barberon M, Caillieux E, Colot V, Jaillais Y, Roudier F, and Vert G. 2016. A versatile Multisite Gateway-compatible promoter and transgenic line collection for cell type-specific functional genomics in Arabidopsis. *Plant J* **85**(2): 320-333.

Nicol JW, Helt GA, Blanchard SG, Jr., Raja A, and Loraine AE. 2009. The Integrated Genome Browser: free software for distribution and exploration of genome-scale datasets. *Bioinformatics* **25**(20): 2730-2731.

Procko C, Crenshaw CM, Ljung K, Noel JP, and Chory J. 2014. Cotyledon-Generated Auxin Is Required for Shade-Induced Hypocotyl Growth in Brassica rapa. *Plant Physiol* **165**(3): 1285-1301.

Wang X Wang H Wang J Sun R Wu J Liu S Bai Y Mun JH Bancroft I Cheng F et al. 2011. The genome of the mesopolyploid crop species Brassica rapa. *Nat Genet* **43**(10): 1035-1039.

Warming S, Costantino N, Court DL, Jenkins NA, and Copeland NG. 2005. Simple and highly efficient BAC recombineering using galK selection. *Nucleic Acids Res* **33**(4): e36.

Zhao C, Craig JC, Petzold HE, Dickerman AW, and Beers EP. 2005. The xylem and phloem transcriptomes from secondary tissues of the Arabidopsis root-hypocotyl. *Plant Physiol* **138**(2): 803-818.